Trans Indian Inst Met (2019) 72(8):2011–2018
https://doi.org/10.1007/s12666-018-1533-3

TECHNICAL PAPER

Conventionally Sintered Hydroxyapatite–Barium Titanate Piezo-Biocomposites

Prabaha Sikder[1] · Naresh Koju[1] · Boren Lin[2] · Sarit B. Bhaduri[1]

Received: 17 August 2018 / Accepted: 4 December 2018 / Published online: 1 January 2019
© The Indian Institute of Metals - IIM 2019

Abstract The central goal of this initial effort is to develop and characterize distinctive piezo-biocomposites as load-bearing orthopedic implants. The motivation is derived from the fact that mammalian bone is a piezoelectric material and this property is helpful in the natural healing of fractured bone. We have employed a cost-effective and industrially viable technique—conventional sintering to consolidate specific compositions of hydroxyapatite (HA) and barium titanate (BT). HA is the primary mineral constituent of mammalian bone but is not piezoelectric. On the contrary, BT is well known for its piezoelectric properties. Their combination creates piezo-biocomposites. The sintering is reactive in nature as BT decomposes into several compounds. Average grain sizes of piezo-biocomposites lie in the range of 1.75–1.9 μm. Interestingly, 15% compressive strength enhancement is noted in the case of HA-40 wt% BT as compared to HA. In vitro examinations reveal favorable bioactivity and biocompatible nature of the composites. These results show that conventionally sintered HA-BT piezo-biocomposites can qualify as candidate materials for load-bearing implants at affordable prices.

Keywords Conventional sintering · Hydroxyapatite · Barium titanate · Orthopedic implants

✉ Prabaha Sikder
james.sikder@gmail.com;
Prabaha.sikder@rockets.utoledo.edu

[1] Department of Mechanical Industrial and Manufacturing Engineering, The University of Toledo, Toledo, OH 43606, USA

[2] Department of Bioengineering, The University of Toledo, Toledo, OH 43606, USA

1 Introduction

Issues related to nonunion of bone fractures cause complexities in 5–10% of 6 million fractures that take place annually in the USA [1]. Other examples of complications in long bone fractures include delayed union and false union [1, 2]. Even though complexities are still a small percentage, the total number of occurrences is still significant. These complications result in additional treatment costs which add $3 billion to $6 billion to medical expenses. A vast number of rest of the fractures do heal without complications due to the piezoelectric nature of the mammalian bones. As early as in 1957, Fukada and Yasuda reported the occurrence of piezoelectric effect in human and bovine femurs [3]. Subsequently, they stated that the polarization of hydrogen bonds within the polypeptide chains of collagen crystals is the origin of the piezoelectric effect [4]. Bassett and Becker, for the first time, reported that the presence of an electric potential influences osteoblast activities and the alignment patterns of macromolecules of the extracellular matrix [5]. Furthermore, Bassett observed enhanced bone growth around the periphery of negatively charged surfaces than positively charged ones of deformed bones [6]. These results meant that the application of external electrical stimulation or a piezoelectric implant could enhance osseous formation. Indeed, with dc electrical stimulation, Fredericks et al. [7] reported a significantly higher gene expression of osteoblasts in a posterolateral spinal model. However, the application of external electric fields to accelerate fracture healing is cumbersome. A better idea to stimulate bone growth is to use a piezoelectric implant into a patient's body.

Of all synthetic orthopedic biomaterials, hydroxyapatite (HA, $Ca_5(PO_4)_3(OH)$) with its similarity to the chemical composition of minerals in hard tissues is an essential

candidate for bone substitutes [8–10]. It is known for its several favorable properties like biocompatibility and non-inflammation and thus is chosen as the primary constituent in the present study [11]. The choice is also dictated by the existing data in the literature. There are several papers in the literature reporting the interesting properties of incorporation of barium titanate (BT, $BaTiO_3$) into HA [8].

Piezoelectric nature and biocompatibility of BT have been well documented in *vivo* [12–16] and in vitro [17–19] examinations for the improvement in interfacial strength, cellular activities, tissue ingrowth and neo-bone formation. As early as 1975, Jianqing et al. [13] conducted a study on canine jawbones using polarized HA-BT and claimed earlier osteogenesis as compared to its bulk HA counterpart. On the contrary, Park et al. [14] observed no substantial difference between polarized and non-polarized dense BT specimens in vivo. In some instances, just particles like castor bean polymer doped with silicon dioxide (SiO_2) or BT and BT nanoparticles (BTNPs) resulted in higher osteogenesis and neo-bone formation [15, 20, 21]. Over the last decade, there is an increase in research on spark plasma sintered (SPS) HA-BT/ HA-calcium titanate (HA-CT) piezo-biocomposites [16, 17, 22, 23]. Dubey et al. [8] reported that HA-40 wt% BT demonstrates physical, electrical and mechanical properties close to the natural bone. Dubey and Basu [17] reported a comparative study of cell proliferation on multistage SPS-ed HA-BT biocomposites when subjected to pulsed electrical stimulation and surface charge generated via electrical poling. Furthermore, Thrivikraman et al. [24] revealed that substrate conductivities of sintered HA-CT biocomposites affect the cell proliferation and differentiation. Even twinning of CT grains plays a vital role in the enhancement of fracture toughness, flexural strength and tensile strength [25]. Recently in 2017, Prakasam et al. [26] reported an enhanced dielectric permittivity of HA-BT sample using single step SPS at temperatures around 850 °C–900 °C and uniaxial pressure of 100 MPa.

Our group has recently reported the development of an injectable, self-hardening, actively smart piezoelectric bone cement based on a different calcium phosphate phase known as monetite. It has BT as the piezoelectric material [27]. Injectable bone cements are best suitable for minimally invasive orthopedic applications [27]. However, their poor mechanical properties limit them in load-bearing applications. While porous HA improves rapid bone ingrowth, dense HA does not have that bioactivity but is essential in load-bearing applications [28]. Accordingly, studies on dense bioceramic product characterization can be a crucial step towards proving their viability in biomedical applications. Sintering technique has been widely implemented for the fabrication of such dense HA products. Among different sintering techniques, currently, spark plasma sintering (SPS) has been the most popular one. This technique promotes densification and decreases sintering temperature and/or time [29]. From a commercial perspective, SPS is capital-intensive and requires expertise; thus, it may not be industrially viable. SPS can also produce simple axisymmetric shapes [30, 31]. On the other hand, conventional pressureless sintering is easy to use, economic and also industrially viable.

The present paper is different from all previous papers in that piezo-biocomposites are sintered for densification. This processing results in different phases and microstructures. It is interesting to compare the properties of such materials with the data on the SPS-ed piezo-biocomposites.

2 Experimental

2.1 Materials and Sample Preparation

Educational grade HA was used in the preparation of samples (Fisher Scientific). Barium titanate (BT, 99.5%, particle size $\leq$ 2 µm) and polyvinyl alcohol (PVA) (87–90%) were purchased from Sigma-Aldrich. Initially, all powders were homogeneously mixed manually using a mortar and pestle. For each 5 gm of HA+BT composition, 0.05 g of PVA was added as a binder. Samples consisting of 0, 20 and 40 wt% BT were prepared. These nominal compositions are represented as HA-x BT in Table 1. 1 g of mixed powder was inserted into a die of ½ inch diameter and uniaxially pressed at approximately 65–70 MPa for 3 min. These compacted pellets were then subjected to the conventional ramp and hold sintering technique inside a conventional sintering furnace (Zircar Zirconia, Inc., Florida, NY). A heating rate of 10 °C/min was used to reach a maximum temperature 1200 °C with a soak of 1 h. Samples were then allowed to cool down to room temperature at the furnace cooling rate. These sintered samples were then subjected to different tests.

2.2 Physical Properties

Bulk densities and apparent porosities of all sintered samples were calculated using standard procedures. The bulk density was calculated with the mass and geometrical

Table 1 Various compositions of sintering samples

Composition	HA (g)	BT (g)	PVA (g)
HA	5.00	–	0.05
HA-20BT	4.00	1.00	0.05
HA-40BT	3.00	2.00	0.05

volume of sintered samples. For calculation of apparent density, samples were initially immersed in the DI water and ultrasonicated for 15 min and subsequently kept immersed overnight to ensure saturation of pores.

2.3 Mechanical Properties

2.3.1 Compressive Strength

Uniaxial compression tests were carried out on samples using a universal testing machine with 50 KN load cell (model 5569, Instron, Norwood, MA, USA). As per the protocol of the American Dental Association, i.e., 0.75 ± 0.25 mm min^{-1}, the crosshead loading rate of 0.5 mm min^{-1} was set [32]. The compressive strength (σ_{max}) of a sample was calculated using the following equations:

$$\sigma_{max} = \frac{P_{max}}{A} \quad \text{and} \quad A = \frac{\pi D^2}{4}$$

where P_{max} is peak load during the test, and A and D are cross-sectional area and diameter of the sample, respectively. The test was conducted in triplicates for each composition.

2.3.2 Hardness and Fracture Toughness

Hardness and fracture toughness values of sintered, mounted and polished samples were evaluated via Vickers microindentation method at a load of 0.5 kg with a dwell time of 10 s. For each sample, ten indentations were made, and the average value was reported as mean ± SD. The Vickers hardness (HV) values were calculated using the standard equation:

$$\text{HV} = 0.001854 \times \frac{P}{d^2}$$

where P is the indentation load and d is the average diagonal length of indentation. The indentation diagonals and crack lengths were measured under SEM.

The Evans and Charles equation [33] was used for the measurement of sample indentation fracture toughness. With the measurement of indentation, half diagonal 'a', crack length 'c' and hardness 'H', the fracture toughness was calculated as:

$$K_{Ic} = 0.16\, Ha^{1/2} \left(\frac{c}{a}\right)^{-3/2}$$

2.4 Physical Characterizations

2.4.1 X-ray Diffraction Analysis

The phase composition analysis of as-prepared sintered HA-x BT samples was carried out with X-ray diffraction (XRD, Ultima III; Rigaku, the Woodlands, TX) with monochromated Cu Kα radiation (44 kV, 40 mA) over a 2θ range of 10°–60° with a continuous scan mode at a speed of 0.75° min^{-1}. All the phases of the sample were determined using the JADE (MDI, Livermore, CA, USA) software.

2.4.2 Fourier Transform Infrared Spectroscopy Analysis

Fourier transform infrared spectroscopy (FTIR, UMA-600 Microscope, Varian Excalibur Series, Digilab, Holliston, MA, USA) was performed on each composition to detect the functional groups present within the sintered samples using an ATR diamond crystal. Within the range of 4000–700 cm^{-1}, 256 scans were performed on each sample.

2.4.3 Morphology of Samples

Scanning electron microscope (SEM, S-4800, Hitachi, Japan) was employed to examine the surface morphologies of as-sintered samples. The samples were mounted on conducting tape and sputter coated before inserting into the SEM vacuum chamber. The grain size of the as-prepared samples was evaluated from SEM micrographs using image J software (developed at the National Institutes of Health). Grain sizes of more than 100 grains were measured, and the average value has been reported.

2.5 Bioactivity of Samples in Simulated Body Fluid (SBF)

For bioactivity evaluation, each sample was immersed in 50 ml of 1.5 × t-SBF at 37 °C for 7 days with the SBF being replenished every 48 h. The 1.5 × t-SBF [34] was prepared by dissolving reagent grade NaCl, $NaHCO_3$, KCl, Na_2HPO_4, $MgCl_2{\cdot}6H_2O$, 1 M HCl, $CaCl_2{\cdot}2H_2O$, Na_2SO_4 and Tris-buffer. At the end of the immersion period, samples were rinsed in DI water and air dried.

2.6 In Vitro Cytocompatibility

All compositions of sintered samples were prepared, autoclaved and immersed in minimum essential medium—Alpha (MEM-α Thermo Scientific, Logan, UT, USA)—with the extraction ratio of 300 mm^2/ml, and were kept at 37 °C and 5% CO_2 for different time frames [35]. MC3T3-E1 osteoblastic cells were also initially seeded in 24-well plates (5×10^4 cells per well) at same 37 °C and 5% CO_2 condition for 24 h. The conditioned medium collected after 24 h was subsequently used to culture the as-prepared MC3T3-E1 cells. After incubating the cells at 37 °C and 5% CO_2 for another 24 h, cells were treated with thiazolyl

blue tetrazolium bromide (MTT, Sigma-Aldrich, St. Louis, MO, USA) for 4 h, insoluble formazan dissolved in DMSO and the optical density was measured at 570 nm wavelength. Non-sintered HA was used as a control. The same procedure was repeated, but this time with a conditioned medium collected after 7 days to culture the cells followed by MTT assay after another 24 h to evaluate the cell viability.

3 Results

3.1 Physical and Mechanical Properties

Figure 1 represents the physical appearance of sintered HA-x BT samples. The indentation made by Vickers microhardness tester and the cracks initiated at the corners are shown in the SEM micrograph in Fig. 2. The bulk density, apparent porosity %, average grain size, compressive strength, Vickers microhardness and fracture toughness of as-prepared samples are given in Table 2. In order to get proper understanding about the efficacy of the present sintering process, we have calculated the % theoretical density or relative density. For HA, the value is approximately 85%. However, relative density decreases for the composites from 66 to 60% with increasing BT concentration. Here, decrease in hardness and toughness values are observed with BT incorporation. The porosity increases with the addition of BT into HA matrix. Furthermore, the compressive strength remains statistically indifferent even with the addition of BT.

3.2 Physical Characterization

3.2.1 XRD Analysis

The XRD patterns of sintered samples are presented in Fig. 3. HA decomposes into α and β-tricalcium phosphate (TCP) phases with the high-temperature soaking and perhaps with the incorporation of BT into samples. Also, the dissociation of BT has resulted in the formation of calcium titanate, tribarium phosphate and dibarium titanate and their intensities increases with the increase in BT content.

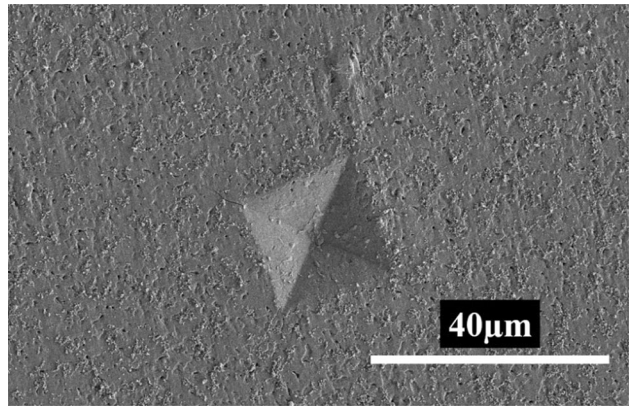

Fig. 2 Cracks initiated from the corners of HA-20BT Vickers indent

The diffraction peaks for HA (JCPDS PDF# 98-000-0251), β-TCP (JCPDS PDF# 97-009-7500), α-TCP (JCPDS PDF# 97-000-0923), BT (JCPDS PDF# 97-002-7969), $CaTiO_3$ (JCPDS PDF# 98-000-0350), Ba_2TiO_4 (JCPDS PDF# 97-002-9389), $Ba_3(PO_4)_2$ (JCPDS PDF# 97-006-9450) are identified during the analysis.

3.2.2 FTIR Analysis

Figure 4 represents the FTIR spectra of HA-x BT sintered samples. Stretching band corresponding to adsorbed water is observed at 3000–3500 cm^{-1} [36, 37]. An intense peak seen at 3571 cm^{-1} is due to the stretching vibration of OH^- functional group. The carbonate v_3 group is identified by peak at 1650 cm^{-1} [38]. Furthermore, the peak for phosphate v_1 functional group is observed at 961 cm^{-1} and the presence of several peaks and shoulder in the range of 900–1200 cm^{-1} corresponds to the phosphate group [36, 38]. The presence of BT can be identified by strong and wide band between 495 cm^{-1} to 850 cm^{-1} [26]. The peak located at the start (700 cm^{-1}) of the FTIR spectra of HA-20/40 BT samples may imply the presence of Ti–O group.

3.2.3 Microstructures of Sintered Samples

The surface microstructures of as-prepared HA-x BT sintered samples are presented in Fig. 5. Smaller grains with

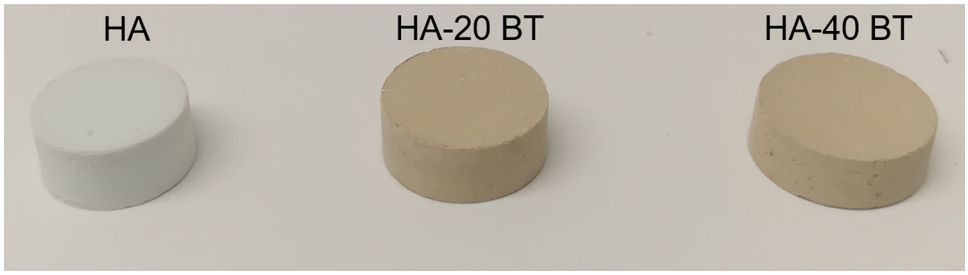

Fig. 1 HA-x BT sintered samples at 1200 °C for 1 h

Table 2 Physical and mechanical properties of HA-x BT samples

Composition	Avg. grain size (μm)	Compressive strength (MPa)	Hardness (GPa)	Toughness (MPa $m^{1/2}$)	Bulk density (g/cc)	Apparent porosity (%)
HA	0.79 ± 0.31	305.68 ± 23.93	3.55 ± 0.19	0.90 ±0.05	2.66 ± 0.02	10.46 ± 0.53
HA-20BT	1.75 ± 0.61	345.46 ± 13.67	2.33 ± 0.15*	0.85 ± 0.04*	2.48 ± 0.07*	22.67 ± 1.75*
HA-40BT	1.95 ± 0.88	350.41 ± 15.28	1.91 ± 0.08*, **	0.80 ± 0.04*, **	2.55 ± 0.04	25.26 ± 0.24*

*Statistically different with HA ($p < 0.05$)

**Statistically different with HA-20 BT ($p < 0.05$)

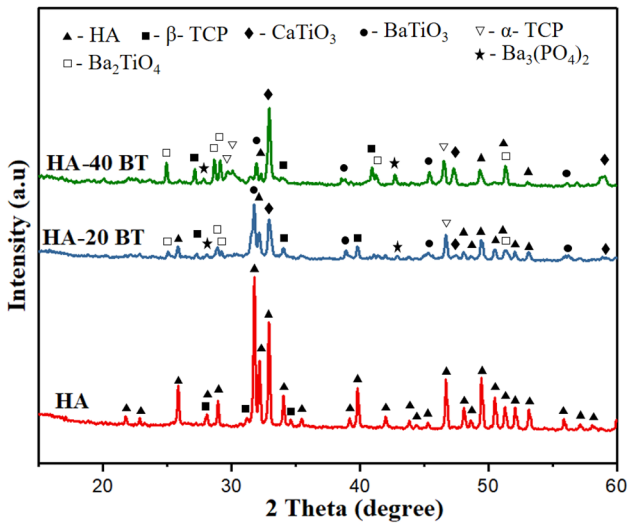

Fig. 3 XRD analysis of sintered HA-x BT samples

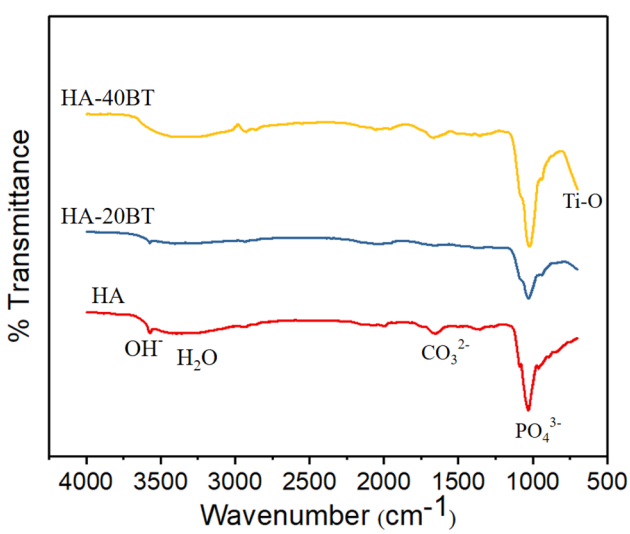

Fig. 4 FTIR absorbance spectrum of sintered HA-x BT samples

average grain size of 0.78 μm are observed on sintered HA samples. However, the grain size distribution range increases with the increase in the BT wt%. In addition, the SEM micrograph shows higher number of blowout holes on the surface of HA samples when compared to the BT incorporated samples.

3.3 Bioactivity of Sintered Samples

After 7 days of immersion of samples in 1.5 × t-SBF, surface morphologies of immersed samples are analyzed under the SEM. All the SBF immersed samples possess globules and flower-like apatite structure (Fig. 6a–c) implying the good bioactivity of sintered samples [39, 40]. The high-magnification SEM image (Fig. 6d) shows the typical petal/flake-like morphological feature of apatite particles [39].

3.4 In Vitro Cytocompatibility

The *in vitro* cell viability results are shown in Fig. 7. No negative effect on the cell viability of sintered samples is observed as compared to the non-sintered HA control after 24 h. To further analyze the extent of cytotoxicity of BT incorporation, the MC3T3-E1 cells are cultured with highly concentrated conditioned media (7 days). All samples display good cell viability regardless of the content of BT.

4 Discussion

The apparent porosity (Table 2) of sintered samples increases from 10.46 to 25.26% with the increase in BT content. This result implies the significant influence of BT on the sintering kinetics and densification of HA-x BT samples. The preparation of a green body with a low pressure is believed to be the major source of porosity. Furthermore, for these sintered piezo-biocomposites, we have observed that Ø HA < Ø HA-20BT < Ø HA-40BT. This suggests that the % shrinkage is highest for only HA and increases simultaneously with the increase of BT wt%. The efficacy of this shrinkage can also be a possible reason behind the lowest porosity of sintered HA samples. The relative density results are in the same accordance with the porosity of the composites. Higher porosity in HA-40BT

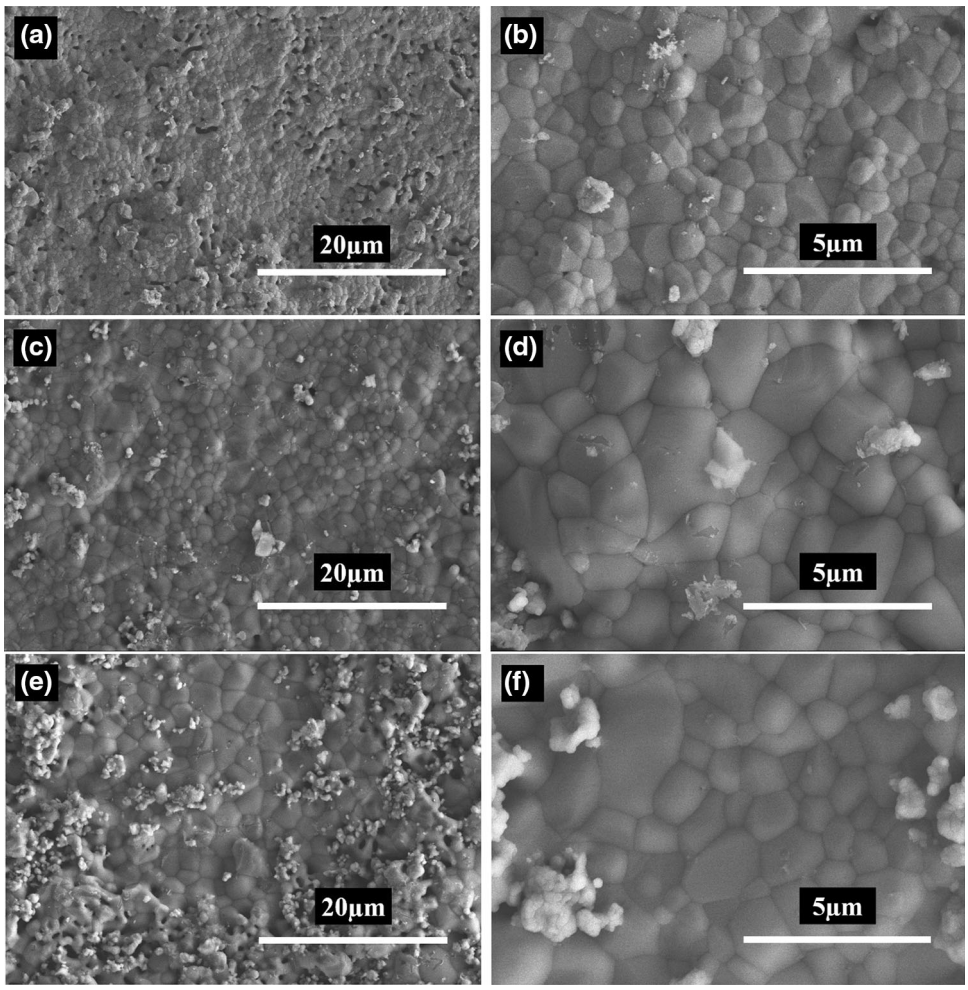

Fig. 5 SEM images of sintered **a**, **b** HA, **c**, **d** HA-20 BT, **d**, **e** HA-40 BT

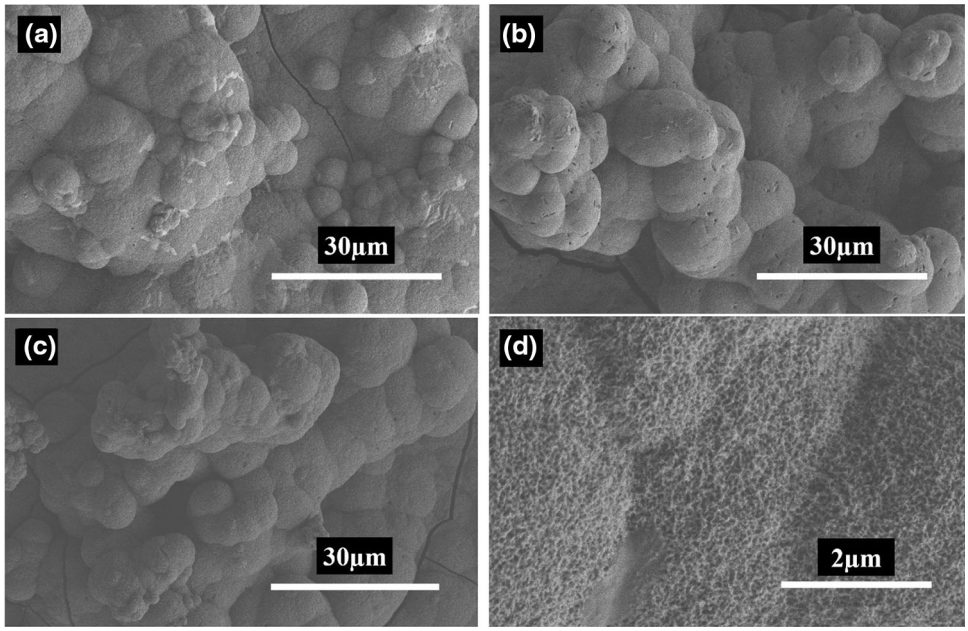

Fig. 6 SEM images of sintered **a** HA, **b** HA-20 BT, **c**, **d** HA-40 BT after 7 days immersion in 1.5 × t-SBF

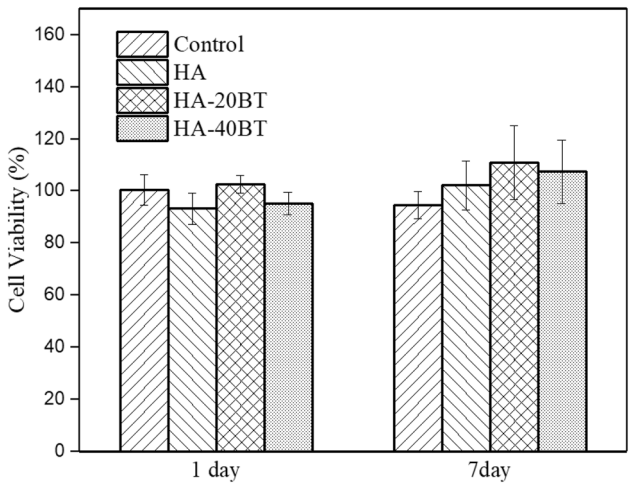

Fig. 7 Cytocompatibility of HA-x BT sintered samples after 1 and 7 days

results in lower relative density as compared to HA-20BT. The higher porosity of HA-20/40BT samples accounts for the lower values of hardness and fracture toughness as compared to monolithic HA samples. Dubey et al. [8] employed SPS technique to prepare HA-BT piezo-biocomposites and reported the compressive strength of HA-40BT to be 138.3 MPa. Later, Dubey et al. [22] developed porous nanophase HA-BT composite with a porosity of approximately 30% and compressive strength of 236 MPa for 25 vol. % BT. In comparison, in our present study, conventionally sintered HA-20/40BT piezo-biocomposites with a porosity of 22–25%, maintain compressive strength within the range of dentine (295 MPa) and enamel (384 MPa) [9]. We can expect lower porosity of our samples by increasing sintering temperature to 1350–1400 °C; however, this increase in sintering temperature will accelerate the decomposition reaction which in turn has a detrimental effect on the physical and mechanical properties of the sintered samples.

The XRD analysis (Fig. 3) of as-sintered HA samples mainly consists of diffraction peaks of HA and few corresponding to β-TCP. However, with the addition of BT into the sample composition, more dissociation of HA occurs. Furthermore, the reactive sintering occurs such that the reaction between HA and BT generates different phases namely α-TCP, β-TCP, CT, $Ba_3(PO_4)_2$ and Ba_2TiO_4. While comparing our conventional sintering results with SPS results from the literature, we can clearly identify that the advanced SPS technique inhibits the decomposition sintering reaction. Prakasam et al. claimed that the sintering temperature increases with the increase in BT content, which in turn causes the decomposition of HA into β-TCP, α-TCP, CT, $Ba_{10}(PO_4)_6$ $(OH)_2$ and loss of OH^- in HA [8, 26]. A small amount of β-TCP in HA implant accelerates its bonding with natural bone [41]. The formation of TCP during sintering enhances in vitro dissolution rate [42]. Thus, with a variation in sintering conditions, contents of TCP within the HA-x BT samples can be varied to achieve an optimum degradation rate and hence a desirable extent of osseointegration. The presence of CT improves the strength, fracture toughness, dielectric properties, conductivity, cell proliferation and differentiation when incorporated within bulk HA sintered biocomposites [24, 25, 42]. Mallik et al. [23] reported 140% increase in de novo osteogenesis at an early stage when HA-80 wt% CT is implanted in rabbit femoral defects as compared to monolithic HA. Therefore, the presence of CT in our final sintered samples is expected to be beneficial in enhancing the cellular activities, growth and differentiation.

The effect of BT addition can also be seen on grain sizes of as-sintered samples. During the conventional sintering of HA, negligible densification occurs below 900 °C, followed by significant densification up to 1150 °C. The SEM micrograph of as-prepared HA-20/40BT samples (Fig. 5c–f) exhibits more extensive range of grain size distribution as they possesses a coarser grain of 2–3.2 μm (HA-20BT), 2–4.5 μm(HA-40BT) and finer grains of 1–2 μm. Dubey et al. (2013) reported the bimodal distribution of grain sizes for conventionally sintered HA-40CT composite [42]. However, in our present study, BT infused samples result in higher number of finer grains along with a normal distribution of grain sizes.

The preliminary assessments of in vitro cytocompatibility and bioactivity are important steps for future in vivo experiments [43]. Negative poling of BT and HA-BT sample surfaces assists in the higher cell proliferation and growth than positively charged and uncharged sample surfaces [16, 19]. On the contrary, Baxter et al. [44] reported insignificant differences regarding in vitro cell adhesion, proliferation and viability on poled and unpoled 90% BT samples after 7 days. In our present work, we have observed the uniform formation of apatite layer on the sample surface after 7 days immersion in 1.5 × SBF. This proves appropriate in vitro bioactivity of as-prepared piezo-biocomposites without poling. Furthermore, the cell viability assay provides a strong indication regarding the feasibility of HA-x BT biocomposite as all sintered samples show no adverse effects on the viability of MC3T3 cells even at higher concentration of media corroborating the non-toxic nature of BT and/or CT. Although the results are not significant, HA-20BT shows slightly higher cell viability than other composition including non-sintered HA control, indicating HA-20BT composition to be an optimum BT wt% in HA samples when conventional sintering is incorporated.

5 Conclusion

The results from the present effort demonstrates the feasibility of conventional sintering of HA-x BT piezo-biocomposites. As opposed to the capital-intensive spark plasma sintering technique, the conventional sintering is economical and is sufficient as a means of fabricating complex shapes beyond the axisymmetric ones. The work shows higher compressive strength and comparable fracture toughness. The dissociation of HA and BT into various phases such as TCP and CT is expected to be advantageous as they may favor the bioactivity, cell responses and dissolution rate of as-sintered composites. Considering physical, mechanical and biological aspects, the conventional sintered HA-BT samples can be a viable alternative for the load-bearing orthopedic applications and demands for the further detailed studies.

Acknowledgements SBB is humbled by being able to contribute to this issue in honor of Prof. E. C. Subbarao. He has many fond memories of interactions during many trips that occurred between DMRL, Hyderabad, and TRDDC, Pune, between years 1983 and 1989. This work was supported by the NSF Grant No. 1706513.

References

1. Simon J, and Simon B, Electrical bone stimulation. In Musculoskeletal Tissue Regeneration Human Press (2008) 259.
2. Carrodeguas R G, V' zquez B, del Barrio J S R, and de la Cal A M, Int J Polym Mater **51** (2002) 591.
3. Fukada E, and Yasuda I, J Phys Soc Jpn **12** (1957) 1158.
4. Fukada E, and Yasuda I, Jpn J Appl Phys **3** (1964) 117.
5. Bassett C A L, and Becker R O, Science **137** (1962) 1063.
6. Bassett C A L, Sci Am **213** (1965) 18.
7. Fredericks D C, Smucker J, Petersen E B, Bobst J A, Gan J C, Simon B J, and Glazer P, Spine **32** (2007) 174.
8. Dubey A K, EA A, Balani K, and Basu B, J Am Ceram Soc **96** (2013) 3753.
9. Akao M, Aoki H, and Kato K, J Mater Sci **16** (1981) 809.
10. Bellucci D, Desogus L, Montinaro S, Orrù R, Cao G, and Cannillo V, J Eur Ceram Soc **37** (2017) 1723.
11. Karimzadeh A, Ayatollahi M R, Bushroa A R, and Herliansyah M K, Ceram Int **40** (2014) 9159.
12. Park J B, Von Recum A F, Kenner G H, Kelly B J, Coffeen W W, and Grether M F, J Biomed Mater Res Part A **14** (1980) 269.
13. Jianqing F, Huipin Y, and Xingdong Z, Biomaterials **18** (1997) 1531.
14. Park J B, Kelly B J, Kenner G H, Von Recum A F, Grether M F, and Coffeen W W, J Biomed Mater Res Part A **15** (1981) 103.
15. Nacer R S, Silva B A K D, Poppi R R, Silva D K M, Cardoso V S, Delben J R J, and Delben A A S T, Acta Cir Bras **30** (2015) 255.
16. Dubey A K, Thrivikraman G, and Basu B, J Mater Sci Mater Med **26** (2015) 1.
17. Dubey A K, and Basu B, J Am Ceram Soc **97** (2014) 481.
18. Grether M F, Coffeen W W, Kenner G H, and Park J B, Biomater Med Devices Artif Organs **8** (1980) 265.
19. Park Y J, Hwang K S, Song J E, Ong J L, and Rawls H R, Biomaterials **23** (2002) 3859.
20. Ciofani G, Ricotti L, Canale C, D'Alessandro D, Berrettini S, Mazzolai B, and Mattol, V, Coll Surf B Biointerfaces **102** (2013) 312.
21. Ciofani G, Danti S, D'Alessandro D, Moscato S, Petrini M, and Menciassi A, Nanoscale Res Lett **5** (2010) 1093.
22. Dubey A K, and Kakimoto K I, Mater Sci Eng C **63** (2016) 211.
23. Mallik P K, and Basu B, J Biomed Mater Res Part A **102** (2014) 842.
24. Thrivikraman G, Mallik P K, and Basu B, Biomaterials **34** (2013) 7073.
25. Ravikumar K, Mallik P K, and Basu B, J Eur Ceram Soc **36** (2016) 805.
26. Prakasam M, Albino M, Lebraud E, Maglione M, Elissalde C, and Largeteau A, J Am Ceram Soc **100** (2017) 2621.
27. Koju N, Sikder P, Gaihre B, and Bhaduri S B, Materials **11** (2018) 1258.
28. Ruys A J, Wei M, Sorrell C C, Dickson M R, Brandwood A, and Milthorpe B K, Biomaterials **16** (1995) 409.
29. Champion E, Acta Biomater **9** (2013) 5855.
30. Sikder P, Sarkar S, Biswas KG, Das S, Basu S, and Das PK, Mater Chem Phys **170** (2016) 99.
31. Sikder P, Pramanick A, Sarkar S, Das S, Dey P P, and Das P K. Adv Appl Ceram **114** (2015) 448.
32. Boroujeni N M, Zhou H, Luchini T J F, and Bhaduri S B, J Biomed Mater Res Part B **102** (2014) 260.
33. Spiegler R, Schmauder S, and Sigl L S, J Hard Mater **1** (1990) 147.
34. Jalota S, Bhaduri S B, and Tas A C, J Mater Sci Mater Med **17** (2006) 697.
35. Sikder P, Koju N, Ren Y, Goel V K, Phares T, Lin B, and Bhaduri S B, Surf Coat Technol **342** (2018) 342.
36. Zhou H, Luchini T J F, Boroujeni N M, Agarwal A K, Goel V K, and Bhaduri S B, Mater Sci Eng C **50** (2015) 45.
37. Sikder P, Grice C R, Lin B, Goel V K, and Bhaduri S B, ACS Biomater Sci Eng **4** (2018) 2767.
38. Rehman I, and Bonfield W, J Mater Sci Mater Med **8** (1997) 1.
39. Sikder P, and Bhaduri S B, J Am Ceram Soc **101** (2018) 2537.
40. Koju N, Sikder P, Ren Y, Zhou H, and Bhaduri S B, Curr Opin Chem Eng **15** (2017) 49.
41. Monmaturapoj N, and Yatongchai C, J Metals Mater Miner **20** (2017).
42. Dubey A K, Mallik P K, Kundu S, and Basu B, J Eur Ceram Soc **33** (2013) 3445.
43. Ren Y, Sikder P, Lin B, and Bhaduri S B, Mater Sci Eng C **85** (2018) 107.
44. Baxter F R, Turner I G, Bowen C R, Gittings J P, and Chaudhuri J B, J Mater Sci Mater Med **20** (2009) 1697.